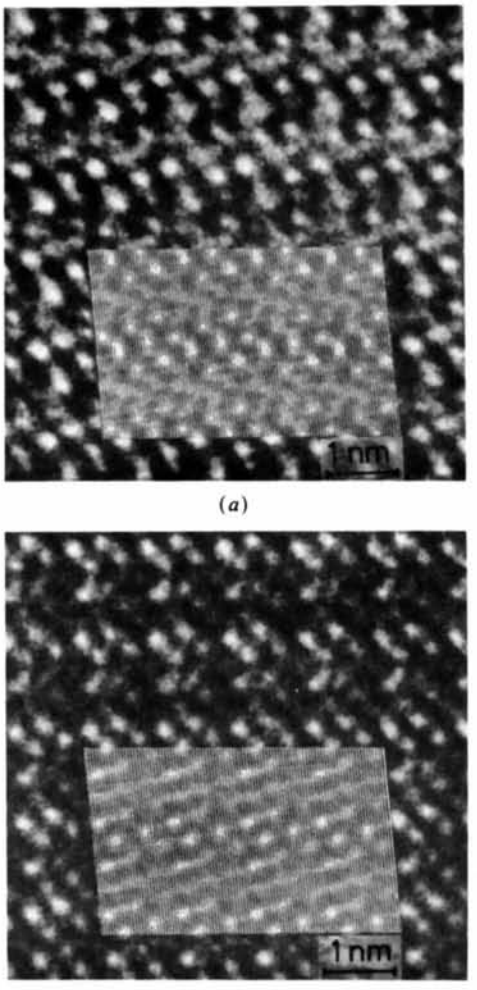

(*a*)

(*b*)

Fig. 10. Observed and calculated images of cebaite. The calculation is carried out assuming the model shown in Fig. 8(*e*). The incident beam is parallel to the *b* axis. Crystal thickness is 50 Å and underfocus (*a*) 200 Å and (*b*) 250 Å.

the proposed model belonging to space group *Cm*. In Table 3 the atomic coordinates of this model are given.

The authors wish to express their gratitude to Professor P. Q. Fu for the valuable mineral samples. Thanks are also due to Assistant Professor H. Endoh, Dr Y. Takai, Messrs N. Ajika, M. Kuwabara, M. Takeda and M. Tomita for their kind help in the calculation and experimental work. FHL would like to thank Professor Z. Z. Peng for constructive discussion.

References

COWLEY, J. M. & IIJIMA, S. (1972). *Z. Naturforsch. Teil A*, **27**, 445–451.

COWLEY, J. M. & MOODIE, A. F. (1957). *Acta Cryst.* **10**, 609–619.

FAN, H. F., ZHANG, R. Y. & ZHAO, G. G. (1963). *Acta Phys. Sin.* **19**, 466–471.

KUMAO, A., HASHIMOTO, H., NISSEN, H.-U. & ENDOH, H. (1981). *Acta Cryst.* A**37**, 229–238.

LI, F. H. & FAN, H. J. (1982*a*). *Acta Phys. Sin.* **31**, 680–684.

LI, F. H. & FAN, H. J. (1982*b*). *Acta Phys. Sin.* **31**, 1206–1214.

LI, F. H., FAN, H. J., YANG, D. Y., FU, P. Q. & KONG, Y. H. (1982). *Acta Phys. Sin.* **31**, 571–576.

LI, F. H., FAN, H. J., ZHANG, P. S. & WANG, Y. H. (1983). *Acta Phys. Sin.* **32**, 460–465.

O'KEEFE, M. A., BUSECK, P. R. & IIJIMA, S. (1978). *Nature (London)*, **274**, 322–324.

PENG, Z. Z. & SHEN, J. C. (1979). *Scientific Papers on Geology for International Exchange Prepared for the International Geological Congress*, pp. 11–18. Beijing, China: Publishing House of Geology.

QIAN, J. Z., FU, P. Q., KONG, Y. H. & GONG, G. H. (1982). *Acta Phys. Sin.* **31**, 577–584.

SCHERZER, O. (1949). *J. Appl. Phys.* **20**, 20–29.

SEMIONOV, E. I. & ZHANG, P. S. (1961). *Kexue Tongbao*, No. 6, pp. 46–48.

SUNDBERG, M. (1978–79). *Chem. Scr.* **14**, 161–166.

TAKAI, Y., HASHIMOTO, H., ENDOH, H. & AJIKA, N. (1981). *EMAG*81, Cambridge, pp. 361–364.

Acta Cryst. (1984). B**40**, 461–465

Structure of the *H* Phase Determined by High-Resolution Electron Microscopy

BY H. Q. YE, D. X. LI AND K. H. KUO

Institute of Metal Research, Academia Sinica, Shenyang, China

(*Received* 27 *January* 1984; *accepted* 18 *May* 1984)

Abstract

A new phase, called *H*, has been found coexisting with the well known σ phase in Fe- and Ni-base superalloys. Owing to an intimate intergrowth of these two phases, a perfect region of *H* never exceeds 10 nm in dimensions. However, its structure was investigated by high-resolution electron microscopy (HREM) and micro electron diffraction and found to be consistent with an interpretation based upon: space group *Cmmm*, $a = 0{\cdot}45$, $b = 1{\cdot}75$, $c = 0{\cdot}45$ nm, $Z = 30$. The atomic positions could easily be fixed owing to the close structure relationship between *H* and σ: $[100]_H \| [4\bar{1}0]_\sigma$, $[010]_H \| [140]_\sigma$, $[001]_H \| [001]_\sigma$.

0108-7681/84/050461-05$01.50

1. Introduction

The tetrahedrally close-packed structures of intermetallic phases of transition metals, which contain only interpenetrating coordination polyhedra with 12 (icosahedron), 14, 15, or 16 vertices and triangular faces, are in most cases generated by the juxtaposing of hexagonal or pentagonal antiprisms. Frank & Kasper (1959) first predicted a hypothetical structure in which the hexagonal antiprisms form 3^34^2 tessellation, quite similar to 3^2434 of the σ phase (Fig. 1). Later, Andersson (1978) called it an untwinned σ phase since it can be generated by intergrowing the same Cr_3Si and Zr_4Al_3 structural units, as can the σ phase, but without the chemical-twinning operation in the latter. In a previous work (Ye & Kuo, 1984) we have shown by HREM that this new phase, named H, coexists together with the σ phase in an Fe-base superalloy [alloy (1) in Table 1]. Moreover, the coexistence of these two phases was further confirmed in an Ni-base superalloy [alloy (2) in Table 1]. In both cases, the perfect region of the H phase seldom exceeds 10 nm in dimensions and Fig. 2 presents a general view of the H phase coexisting with σ. In this high-resolution image, taken under favourable imaging conditions as described in §2, each bright spot may be taken to represent a hexagonal antiprism and the 3^34^2 as well as 3^2434 tessellations of the H and σ phases respectively can be clearly seen.

On account of the smallness of the H crystallite, its structure determination has to rely upon HREM and selected-area electron diffraction (down to linear dimension of 10 nm or even less). However, this is greatly facilitated by the close relationship between the structures of H and σ phases. In this paper the crystal structure of the H phase and its relationship to other tetrahedrally close-packed structures are presented. The domain structures of the H phase will be published elsewhere (Li, Ye & Kuo, 1984).

2. Structure determination

The H phase was found in the σ phase separated from two superalloys. The chemical compositions of the alloys and the σ phases, with a small fraction of H phase in the latter, are shown in Table 1. Since the H phase cannot be separated alone, its composition has not been determined directly. Owing to the close structural relationship between H and σ phases, as demonstrated below, they might be expected to have a similar composition.

The σ phase was extracted electrolytically from these superalloys in an electrolyte consisting of 3% $FeSO_4$, 3·5% H_2SO_4, 2% $NaNO_3$ in water at 282–284 K with a current density of 3–10 mA cm^{-2}. High-resolution images were taken in a JEM 200CX electron microscope having an objective lens with C_s = 1·2 mm. The objective-aperture size used corresponded to about 7 nm^{-1} in reciprocal space. The point resolution, as defined by the first zero in the transfer function at Scherzer defocus, is about 0·25 nm.

The computer image simulation was carried out using the multislice program written by Ishizuka (1982) including first- and second-order partial coherent envelopes. The image simulation was first carried out on the well known σ phase (Ye & Kuo, 1984). Our calculation has shown that the phases of the major diffracted beams (200, 210, 140, 330 *etc.*), having higher intensities and thus making more important contributions to the final image, may vary from 0 to π when the crystal thickness increases from 0 to 5 nm. This variation is large enough to destroy an ideal structural image. It is clear that the image will change rapidly with thickness and also with defocus value so that careful image matching will be required to ascertain the best imaging conditions. From the point of view of kinematical diffraction, $\frac{1}{4}\xi_{000}$ (4 nm, about 8 slices) and $\frac{3}{4}\xi_{000}$ (10 nm, about 20 slices) were chosen as the crystal thicknesses, which correspond to the two sides of the first *Pendellösung* fringe (dark band) in the experimental images. The defocus values −70

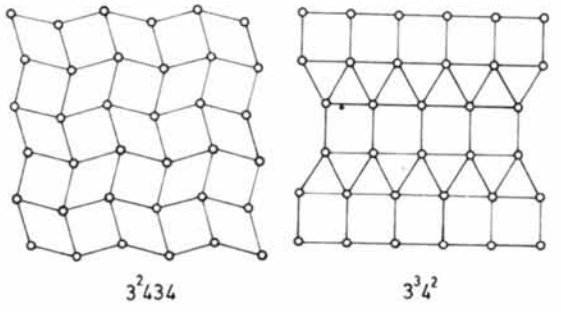

Fig. 1. 3^2434 and 3^34^2 tessellations of hexagonal antiprisms, represented by circles, in σ and H phases respectively, after Frank & Kasper (1959). Note they have the same zigzag sheets in the vertical direction.

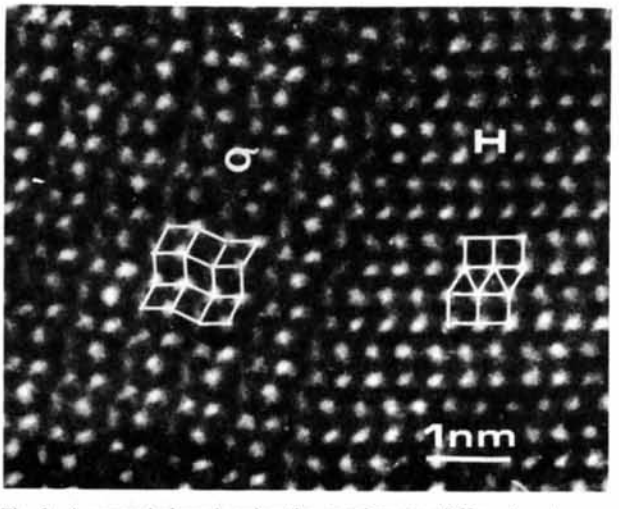

Fig. 2. A general view showing the coexistence of H and σ phases, the bright spots of the former constituting a 3^34^2 net whereas those of the latter constitute a 3^2434 one (*cf.* Fig. 1).

Table 1. *Compositions of superalloys and σ phase* (wt%)

	Cr	Ni	W	Mo	Al	Ti	Fe	C	B
Alloy No. (1)	15	35	2	2	2·4	2·3	Balance	0·04	0·01
σ	29·5	11·1	7·7	9·5	—	—	42·5	(a = 0·881, c = 0·458 nm)	

	Cr	Ni	W	Mo	Al	Ti	Fe	Co	C	B
Alloy No. (2)	8·7	Balance	—	3·05	6·25	5·68	0·35	10·2	0·44	0·016
σ	44·8	13·7	—	9·6	1·6	1·6	3·6	25·1	—	—

Table 2. *Parameters for computer-simulation image*

Electron wavelength (nm)	$2{\cdot}51\times10^{-3}$
Spherical-aberration constant (mm)	1·2
Incident-beam divergence (rad)	$0{\cdot}75\times10^{-3}$
Defocus due to chromatic aberration (nm)	7
Objective-aperture radius (nm^{-1})	7
Crystal thickness for one slice (nm)	0·45

and −130 nm corresponding to two broad bands in the transfer function were used. The half-width of a Gaussian spread of defocus can be estimated from the variances in the statistically independent fluctuations of accelerating voltage and objective-lens current, and also from the energy distribution of electrons, leaving the gun filament, which is in turn controlled by the electron-gun bias setting. The beam divergence can be obtained from a focused second condenser aperture diffraction pattern. The parameters used in the image simulation are shown in Table 2. The bright spots forming a network of 3^2434 in the experimental images of the σ phase can be obtained in the first broad frequency band with a thickness of 4 nm and in the second band with a thickness of 10 nm (Ye & Kuo, 1984). Though the 3^2434 network shows only the arrangement of the hexagonal antiprisms, it is clear enough to demonstrate the structural characteristics of the σ, H, Zr_4Al_3, and Cr_3Si structural units. In our experimental images, the half-width of a Gaussian spread of defocus, the semiangle of convergence and the size limited by the objective aperture were all kept in the same conditions and can be measured experimentally. The main factors affecting the image appearance are the crystal thickness and defocus values. According to our results of image simulation (Ye & Kuo, 1984), the images taken along the thinner side of the first *Pendellösung* dark band at Scherzer defocus and those taken at the thicker side of the first *Pendellösung* fringe at second broad band defocus both showed the same characteristics, *i.e.* the tunnel inside the hexagonal antiprism was resolved as a bright spot.

Fig. 3 shows a high-resolution image of the H phase taken near the thicker side of the first *Pendellösung* fringe with a defocus of −130 nm. The distance between two bright spots in the image is approximately 0·45 nm, being the same as in the σ phase. It is reasonable to assume that the bright spots in the image of the H phase also correspond to the hexagonal antiprisms (the simulated image will be discussed below). In order to ascertain the arrangement of the hexagonal antiprisms in the H phase, it is of interest to examine the arrangement of hexagonal antiprisms in the σ and H phases in a high-resolution image (see Fig. 2). In the tetragonal σ phase, four hexagonal antiprisms form a square Cr_3Si unit. The atomic arrangement in the σ phase projected along [001] can be described as consisting of 28°-rotation square units sharing corners thus generating rhomb units of Zr_4Al_3 among them. In the H phase both these square and rhomb units share edges and form separate slabs. Fig. 4 is a schematic diagram of the arrangement of hexagonal antiprisms in the σ and H phases. It can be regarded as a rough model of a structure which might give the image shown in Fig. 2.

The HREM image of the H phase (Fig. 3) exhibits *mm* symmetry and a centred rectangle should be chosen as the two-dimensional cell. Considering the similar mode of juxtaposing hexagonal antiprisms in tetrahedrally close-packed H and σ phases, the third parameter of the H phase should be the same as the c parameter of the σ phase which also has a mirror plane perpendicular to it. It should be noted that, in the (001) projection of the σ phase, the edges of the square Cr_3Si units are parallel to the ⟨140⟩ directions. Thus with this suggested interrelationship between

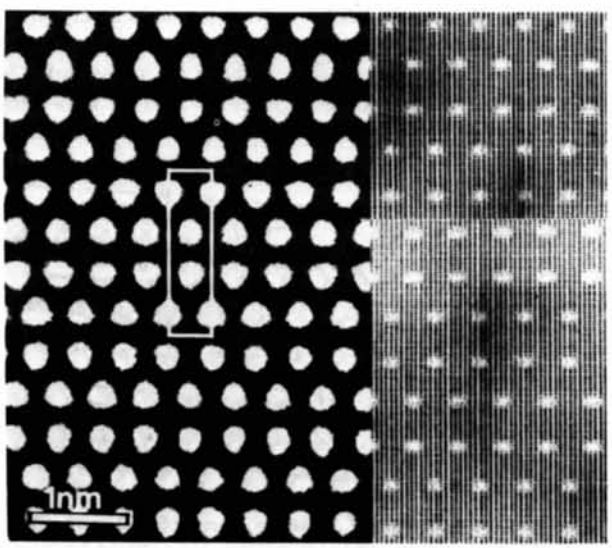

Fig. 3. High-resolution and simulated images of the H phase, each bright spot corresponding to a hexagonal tunnel inside a column of hexagonal antiprisms. The H unit cell is outlined.

the two structures, it can be seen from Fig. 4 that:

$$[100]_H \| [4\bar{1}0]_\sigma, \quad a_H = a_\sigma/2 \cos 14{\cdot}03°$$
$$[010]_H \| [140]_\sigma, \quad b_H = 2a_\sigma \cos 14{\cdot}03° \qquad (1)$$
$$[001]_H \| [001]_\sigma, \quad c_H = c_\sigma$$

where 14·03° is the angle between $[100]_\sigma$ and $[410]_\sigma$. On this basis the H and σ phases have the same unit-cell volume. Hjerten, Marinder, Salwën & Werner (1982) and Self, O'Keefe & Stobbs (1983) have recently discussed the effect of a slight distortion of the secondary layers in the σ phase on its space group. But this distortion is too small to be noticed by HREM. Given the tetragonal structure data of the σ phase (space group $P4_2/mnm$ or $P4_2nm$ with an m perpendicular to the c axis, $a = 0{\cdot}891$, $c = 0{\cdot}45$ nm, $Z = 30$) and the supposed common basis of the H phase as inferred here, the space group of H should be $Cmmm$, $a = 0{\cdot}45$, $b = 1{\cdot}75$, $c = 0{\cdot}45$ nm, $Z = 30$. An orthorhombic rather than tetragonal cell is chosen for the H phase, despite $a = c$, because of its C centre and mmm symmetry. All the atomic parameters and the coordination numbers, are inferred, as in Table 3, on the basis of the arrangement of the hexagonal antiprisms and the supposed symmetry of the structure.

It should be noted that the lattice parameters of the H phase should be related to those of the σ phase and the data listed in Table 3 have not been determined directly. The atom species in the H phase are still unknown, since it is difficult, if not impossible, to determine its composition independently. Since all the coordination relationships remain potentially the same as those in the σ phase, no calculation of the atomic distances was made for the H phase.

Figs. 5(a) and 5(b) show projections of the H phase along the [001] and [100] directions, respectively, with the main symmetry elements shown.

Owing to the very small size of the H-phase particle and the intimate intergrowth of H and σ, it is very hard to obtain its electron diffraction pattern alone.

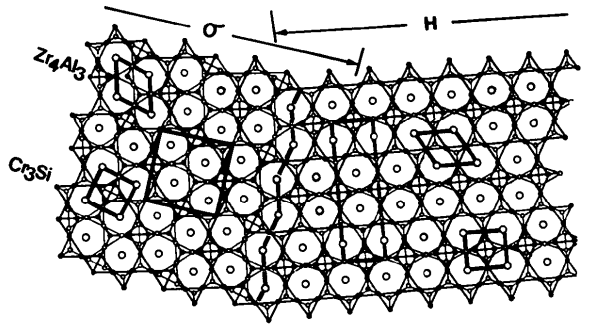

Fig. 4. Structure models of H and σ phases. Small open circles are atoms at $z = 0$ and small filled circles at $\frac{1}{2}$, forming hexagonal antiprisms with atoms (large circles) at $\pm\frac{1}{4}$ inside them. There is a continuous transition from one structure to another without any disorder at the boundary.

Table 3. *Crystallographic data for the H phase*

$Cmmm$ (D_{2h}^{19}); $a = 0{\cdot}45$, $b = 1{\cdot}75$, $c = 0{\cdot}45$ nm; $Z = 30$. Atomic coordinates: $000 + \frac{1}{2}\frac{1}{2}0$.

Type	Number	Position	Coordination number	Coordinates
A	2	2(a)	12	000
B	4	4(e)	12	$\frac{1}{4}\frac{1}{4}0$
C	4	4(i_c)	15	$0y_C0$; $y_C \simeq 0{\cdot}2892$
D	4	4(i_d)	14	$0y_D0$; $y_D \simeq 0{\cdot}4206$
E	4	4(j)	12	$0y_E\frac{1}{2}$; $y_E \simeq 0{\cdot}3677$
F	4	4(h)	14	$x0\frac{1}{2}$; $x \simeq 0{\cdot}2000$
G	8	8(n)	14	$0y_Gz$; $y_G = \frac{1}{8}$, $z = \frac{1}{4}$

Fig. 6(a) is a composite electron diffraction pattern of the H phase and two 28° rotation domains of the σ phase in [001] orientation. Fig. 6(b) is the corresponding indexing diagram where only the diffraction spots of the H phase are indexed since the diffraction patterns of these two σ domains can be recognized without any difficulty by the solid and dotted nets drawn in Fig. 6(b). The positions and intensities of the $hk0$ spots are consistent with the C centre and mm symmetry of the [001] projection of the H phase. They also agree with the parameters a and b given above.

Using the atomic positions given in Table 3, intensities of $hk0$ reflections of the H phase have been calculated using Ishizuka's (1982) multislice program. The maximum indices of the calculated diffraction beams are ±16 for $h00$ and ±32 for $0k0$. The outermost region of calculated dynamical structure factors in reciprocal space is 7 nm^{-1}. The diffracted beams having lower indices show a similar relationship of amplitudes vs thickness. The results from a thickness of 7 nm, as an example, are shown in Fig. 6(b). The sizes of the diffraction spots of the

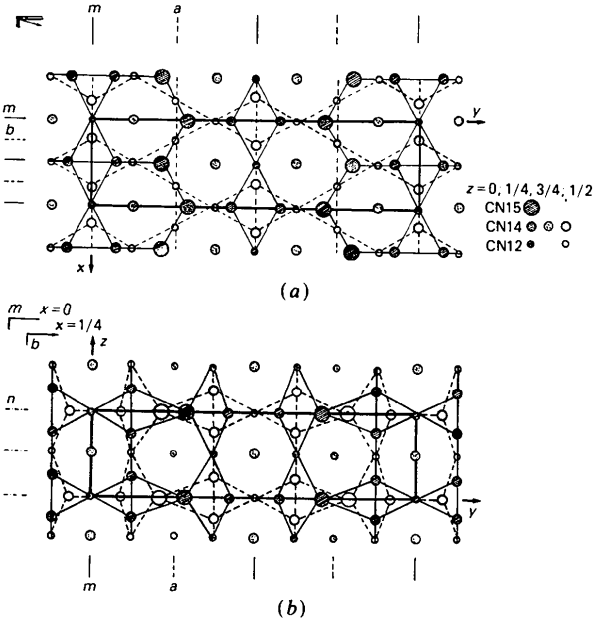

Fig. 5. Projections of the H structure on (a) (001) and (b) (100).

H phase in Fig. 6(b) correspond to five grades of normalized calculated intensities. The calculated values agree quite well with the experimental ones (see Fig. 6a).

A calculation of dynamical structure factors showed that the increment in thickness between two bright-field *Pendellösung* fringes in the case of the H phase is about 9 nm. The thickness parameters, therefore, were chosen as $\frac{1}{4}\xi_{000}$ (4 nm, about 8 slices) and $\frac{3}{4}\xi_{000}$ (12 nm, about 28 slices) respectively. The image simulation also showed that the bright spots forming a network of 3^34^2 can be obtained in the Scherzer defocus with a thickness of 4 nm and in the second broad frequency band of the transfer function with a thickness of 12 nm. A simulated image of a crystal 12 nm thick, using the data listed in Tables 2 and 3, is shown in Fig. 3 which again confirmed a one-to-one correspondence between the bright spots in the high-resolution image and the hexagonal antiprisms in the structure.

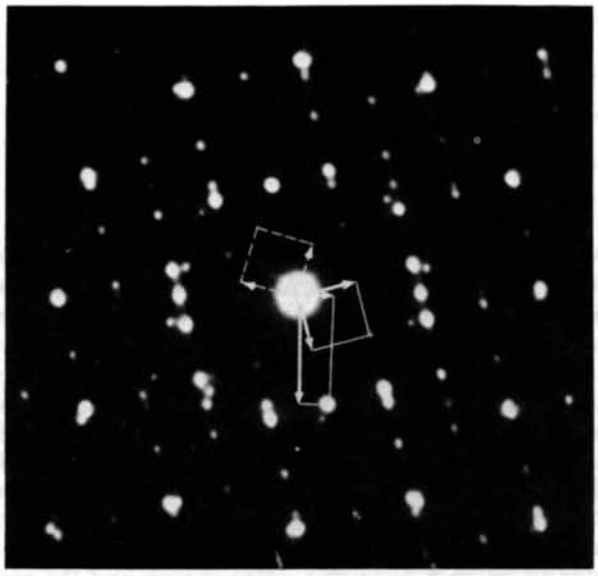

(a)

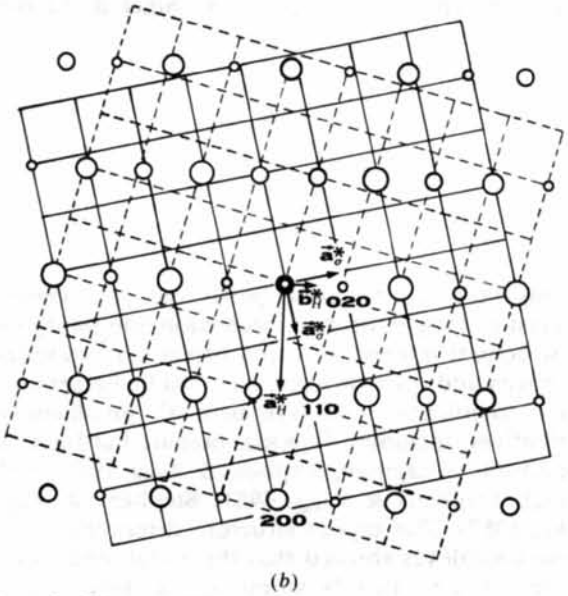

(b)

Fig. 6. [001] Electron diffraction patterns of H and two 28° rotation domains of σ (a); only the spots of H are indexed with the reciprocal lattices of the two σ domains drawn as square nets (b). The size of the circles shows the relative intensities calculated from the H structure.

3. Discussion

The H phase was always found to coexist with the σ phase in the precipitates electrolytically extracted from the two superalloys investigated, at a particle size normally limited to about 10 nm. Obviously, it is impossible to determine its structure by X-ray diffraction analysis. The presence of the phase would also be overlooked by diffraction contrast microscopy at medium magnification. The HREM technique can however readily demonstrate the presence of the phase and give considerable information on its structure.

Several research groups have investigated the σ phase and its planar faults before by means of HREM (Ishimasa, Kitano & Komura 1980*a*,*b*, 1981; O'Keefe, Self, Southwick & Stobbs, 1980; Self, O'Keefe & Stobbs 1983; Stenberg & Andersson, 1979), but none have reported the H phase. Perhaps the H phase is not stable in melted σ phase or in simple alloys. The σ phase precipitated in complex alloys like superalloys is quite different from that studied by the above-mentioned authors in composition, formation temperature and crystallization state, as evidenced by the presence of a high density of various kinds of crystalline defects (Ye & Kuo, 1984; Li, Ye & Kuo, 1984). Therefore, HREM studies made on various precipitates in alloys may be a fruitful route to study the fine structure of this type of alloy phase.

References

ANDERSSON S. (1978). *J. Solid State Chem.* **23**, 191–204.

FRANK, F. C. & KASPER, J. S. (1959). *Acta Cryst.* **12**, 483–499.

HJERTEN, I., MARINDER, B-O., SALWÉN, A. & WERNER, P.-E. (1982). *Acta Chem. Scand. Ser. A*, **36**, 203–206.

ISHIMASA, T., KITANO, Y. & KOMURA, Y. (1980*a*). *J. Solid State Chem.* **36**, 74–80.

ISHIMASA, T., KITANO, Y. & KOMURA, Y. (1980*b*). *Jpn. J. Appl. Phys.* **19**, L483–L486.

ISHIMASA, T., KITANO, Y. & KOMURA, Y. (1981). *Phys. Status Solidi A*, **66**, 703–715.

ISHIZUKA, K. (1982). *Acta Cryst.*, A**38**, 773–779.

LI, D. X., YE, H. Q. & KUO, K. H. (1984). *Philos. Mag.* In the press.

O'KEEFE, M. A., SELF, P. G., SOUTHWICK, P. D. & STOBBS, W. M. (1980). *Electron Microscopy* 1980. Proc. EUREM 80, edited by P. BREDERON & G. BOOM, pp. 264–265. Seventh European Congress on Electron Microscopy Foundation, Leiden.

SELF, P. G., O'KEEFE, M. A. & STOBBS, W. M. (1983). *Acta Cryst.* B**39**, 197–209.

STENBERG, L. & ANDERSSON, S. (1979). *J. Solid State Chem.* **28**, 269–277.

YE, H. Q. & KUO, K. H. (1984). *Philos. Mag.* In the press.

Acta Cryst. (1984). B40, 466–473

pH Dependence of Binding Site in Complexation of Cu^{II} with Picolinamide Groups: Crystallographic Studies of Mono- and Binuclear Complexes with *N,N'*-Dipicolinoyl-1,3-propanediamine*

BY SEI TSUBOYAMA, TOSIO SAKURAI AND KIMIKO KOBAYASHI

The Institute of Physical and Chemical Research (Rikagaku Kenkyusho), Wako-shi, Saitama 351, *Japan*

NAGAO AZUMA

Faculty of General Education, Ehime University, Matsuyama, Ehime 790, *Japan*

AND YUJI KAJIKAWA AND KAZUHIKO ISHIZU

Department of Chemistry, Faculty of Science, Ehime University, Matsuyama, Ehime 790, *Japan*

(*Received* 7 *November* 1983; *accepted* 29 *March* 1984)

Abstract

Three related copper complexes (*a*) $[Cu(C_{15}H_{14}N_4O_2)(H_2O)].2H_2O$, $M_r = 399{\cdot}90$, monoclinic, $P2_1/c$, $a = 11{\cdot}730\ (5)$, $b = 13{\cdot}097\ (7)$, $c = 12{\cdot}668\ (5)$ Å, $\beta = 119{\cdot}59\ (3)°$, $U = 1692\ (1)$ Å^3, $Z = 4$, $D_m = 1{\cdot}59$, $D_x = 1{\cdot}570$ Mg m^{-3}, $T = 296$ K, final $R = 4{\cdot}6\%$ ($wR = 5{\cdot}4\%$) for 2279 independent reflections; (*b*) $[CuCl(C_{15}H_{16}N_4O_2)]_2SO_4.8H_2O$, $M_r = 1006{\cdot}82$, monoclinic, $P2_1/c$, $a = 14{\cdot}679\ (2)$, $b = 13{\cdot}070\ (2)$, $c = 23{\cdot}958\ (6)$ Å, $\beta = 111{\cdot}56\ (2)°$, $U = 4275\ (2)$ Å^3, $Z = 4$, $D_m = 1{\cdot}53$, $D_x = 1{\cdot}564$ Mg m^{-3}, $T = 296$ K, final $R = 6{\cdot}1\%$ ($wR = 6{\cdot}6\%$) for 5415 independent reflections; and (*c*) $[Cu(SO_4)(C_{15}H_{16}N_4O_2)]_2.13H_2O$, $M_r = 1122{\cdot}06$, orthorhombic, $C222_1$, $a = 15{\cdot}42\ (1)$, $b = 24{\cdot}92\ (2)$, $c = 25{\cdot}73\ (2)$ Å, $U = 9885\ (13)$ Å^3, $Z = 8$, $D_m = 1{\cdot}52$, $D_x = 1{\cdot}51$ Mg m^{-3}, $T = 296$ *K*, were studied. In the monomeric complex (*a*) prepared in an alkaline solution, the Cu^{II} ion is surrounded by four N atoms of the two deprotonated amide and two pyridine moieties, and a water molecule at the apex, yielding a distorted square-pyramidal structure. Both complex cations in the dimeric complexes (*b*) and (*c*) obtained in acidic solution have approximate D_2 symmetry, the Cu^{II} ions being surrounded by the two N in pyridine rings and two amide O atoms in each half of two picolinoyl groups in an approximate plane, and two Cl^- ions for (*b*) and SO_4^{2-} ions for (*c*) occupying axial positions respectively. These structures are essentially consistent with those proposed from absorption and ESR studies.

Introduction

In a previous communication, the unique properties of *N,N'*-di(picolinoyl)-1,3-propanediamine [(1), H_2ppda] as a ligand were discussed (Kajikawa, Mukai, Ishizu & Ojima, 1981). This potentially tetradentate amide reacts with copper(II) sulfate in alkaline solution to give a dark blue–violet CuN_4-type complex (Ojima, 1967). The color changes reversibly to blue upon acidification of the solution. The blue complex has been characterized by spectral studies as the dimeric CuN_2O_2 form having a spin triplet state. Particularly for the latter, the ESR study showed that the two equivalent Cu atoms stack together so that the *g* and *D* tensor axes coincide with each other and the distance between two metal ions was evaluated to be *ca* 4 Å. Such a color change and the pH dependence of the binding site are characteristic of biuret, polypeptides or proteins (Sigel & Martin, 1982).

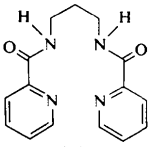

(1)

This investigation arose partly out of a general interest in copper–protein interaction and partly out of structural interest in a spin triplet Cu^{II} complex. Stephens and his coworkers have studied a series of Cu^{II} complexes with symmetrical picolinamide derivatives, including H_2ppda, prepared at high pH conditions (Chapman, Stephens & Vagg, 1980, 1981; Mulqi, Stephens & Vagg, 1981; Stephens & Vagg, 1981, 1982). The crystal structure determination of these complexes showed that the metal atoms were coordinated by two N atoms of the deprotonated amide and two N atoms of the pyridine moiety in all cases. For [Cu(ppda)] two different crystalline forms designated α and β were separated and the structure of the latter has been determined by Stephens & Vagg

* IUPAC name: *N,N'*-trimethylenedi-2-pyridinecarboxamide.

0108-7681/84/050466-08$01.50